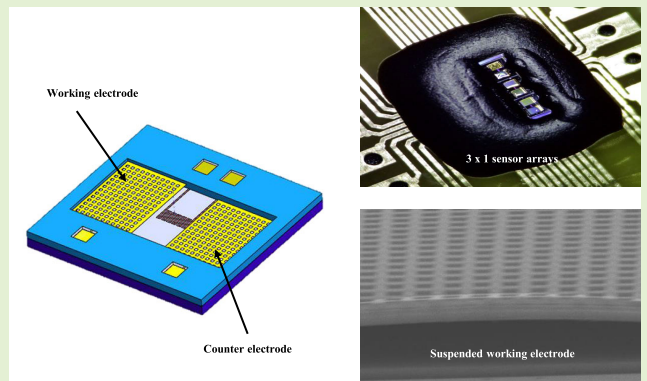


A Miniaturized CMOS-MEMS Amperometric Gas Sensor for Rapid Ethanol Detection

Do Thi Thu, Zong-Han Liu, Ya-Chu Lee¹, Tzu-Wen Kuo, Wei-Lun Sung, Yen-Chang Chu, Yu-Lun Chueh, *Senior Member, IEEE*, and Weileun Fang², *Fellow, IEEE*

Abstract—This study presents the design and implementation of a chip-scale amperometric ethanol sensor using the standard commercially available complementary metal oxide semiconductor (CMOS) process together with the post-CMOS micromachining processes. The presented amperometric sensor consists of a suspended plate with a microhole structure as the working electrode, a fully anchored plate with a microhole structure as the counter electrode, and a microcavity as the electrolyte reservoir. The metal and dielectric layers inherent in the standard CMOS process are exploited to realize these structures. The electrode with a microhole structure could enhance its surface area to improve the sensitivity of the sensor. The suspended working electrode covered a thinner Nafion[®] layer could facilitate gas diffusion to shorten the response time of the sensor. To characterize the ethanol sensing, a Ni film is deposited on the working electrode. Measurements indicate the presented sensor has a sensing range of ppm (20–1000 ppm) at room temperature. Moreover, its sensitivity and response time are, respectively, 0.01 nA/ppm and 6 s. The presented design shows the CMOS-MEMS is a promising approach to realize the amperometric ethanol sensor.

Index Terms—Amperometric gas sensors, complementary metal oxide semiconductor (CMOS)-MEMS, electrochemical (EC) gas sensors, ethanol detection.



I. INTRODUCTION

THERE is growing interest in the detection of exhaled human breath to analyze various diseases, such as asthma, lung cancer, kidney disease, diabetes, and so on [1]. Exhaled breath is composed of nitrogen, oxygen, carbon dioxide, carbon monoxide, nitric oxide (NO), water vapor, and a mixture of volatile organic compounds (VOC), such as hydrocarbons, alcohols, terpenes, aldehydes, and other nonvolatile molecules [2]. Exhaled ethanol concentrations in healthy individuals are typically less than 380 ppb but can reach up to 2300 ppb in patients with liver disease [3]. Moreover, ethanol is a harmful chemical that has to be monitored in various fields, such as food industry,

pharmaceutical, biomedical, biochemistry, beverage industry, and so on [4], [5], [6]. Typically, continued exposure to ethanol vapor may cause severe skin irritation, sore throat, and respiratory damage, even at a low ethanol concentration of 25 ppm [7]. Therefore, it is important to develop a miniaturized gas sensor to quickly detect ethanol from the air environment, as well as exhaled human breath for public safety and health care applications.

The semiconductor and micromachining technologies are promising approaches to offer various advantages for gas sensors, such as the physical size, accuracy, cost, power consumption, and so on [8], [9], [10], [11]. The micromachined gas sensors have been extensively applied in various fields, such as environmental alert [12], food quality [13], medical instruments [14], process control [15], and so on. For example, gas sensors have been developed to monitor toxic/hazardous gases, explosive gases, and air pollution [16], [17], [18]. The gas sensor has also been exploited to analyze diseases from human breathing [19]. To date, various gas-sensing techniques, such as the metal oxide semiconductor (MOS) [20], the surface acoustic wave [21], the optical techniques [22], and the electrochemical (EC) techniques [23], [24] have been reported. Among the existing techniques, the amperometric gas sensor, which adopts the EC sensing approach, exhibits

Manuscript received 2 February 2023; accepted 5 March 2023. Date of publication 14 March 2023; date of current version 14 April 2023. This work was supported in part by the National Science and Technology Council of Taiwan under Grant NSTC 111-2218-E-007-014-MBK. The associate editor coordinating the review of this article and approving it for publication was Prof. Shaibal Mukherjee. (*Corresponding author: Weileun Fang.*)

The authors are with the Department of Power Mechanical Engineering, Department of Materials Science and Engineering, Institute of NanoEngineering and MicroSystem, National Tsing Hua University, Hsinchu 30013, Taiwan, and also with PixArt Imaging Inc., Hsinchu Science Park, Hsinchu 30076, Taiwan (e-mail: fang@pme.nthu.edu.tw). Digital Object Identifier 10.1109/JSEN.2023.3254881

several advantages, including low power consumption, high selectivity, good sensitivity, and low cost [25], [26], [27].

Many approaches, such as electrolyte materials, fabrication technology, and so on, have been investigated to develop a miniaturized monitoring device and further a fast response sensor to enable real-time measurement [28], [29], [30]. For instance, electrolytes, such as ionic liquid (IL) and solid polymer, have been extensively adopted in sensors recently for size reduction and performance enhancement [31], [32]. The IL electrolyte, however, has concerns of moisture interference, slow gas diffusion, and relatively high cost causing considerable limitations of performance and size for sensors [32], [33]. Solid polymer electrolyte, such as Nafion, has shown good conductivity, high gas permeability, and low cost; hence, it has been used both as the electrolyte and support material for electrode structure to improve sensor performance [34], [35]. The process of fabricating microporous sensing electrodes has been developed to realize the miniaturized amperometric NO gas sensor [36]. The microporous electrode is then coated with the Nafion dispersion to achieve a fast response time and high sensitivity (in ppb-level). Additional nonbatched assembly processes and the centimeter scale sensor size are, however, the two concerns for this design. The process of depositing platinum (Pt) on flexible porous polytetrafluoroethylene (PTFE) substrate as the sensing electrode and then employing RTIL as the electrolyte has been introduced [37] to realize the miniaturized gas sensor for rapid measurement of multiple gases. The concept has also been extended to the complementary MOS (CMOS) monolithic gas sensor microsystem to address the power, size, and cost requirements for wearable environmental monitoring devices [38]. The performance of the sensor is limited by the planar structure, and the moisture interference of RTIL electrolytes is another concern. To date, the CMOS processes have become mature fabrication technologies in many commercial foundries. The standard CMOS platform could offer several dielectric, metal, and poly-silicon layers. By adding the post-CMOS micromachining processes, various sensing units, auxiliary structures, and electrical routings can be fabricated and monolithically integrated to realize gas sensors [39]. Thus, a miniaturized amperometric gas sensor can be realized by using the standard CMOS platform. To detect ethanol gas in real-time measurement, a sensing material layer will be deposited on the sensing area via the post-CMOS process.

Many catalyst materials have been used to improve the electrocatalyst activity to ethanol oxidation in fuel cell sensors, including Pt, Pd, W, and Ni [40], [41], [42], [43]. Among these materials, Ni-based electrodes have attracted attention due to their low cost and good EC properties for ethanol oxidation, which have promising prospects in the application of ethanol detection [43]. For example, the Ni aerogel with Ni(OH)₂ hybrid has a current density of 27.6 mA/cm² for ethanol oxidation [44]. The Ni can also dope with some sensing materials, such as SnO₂, In₂O₃, and MoS₂, to enhance its ethanol sensing properties [45], [46], [47]. Therefore, Ni film is integrated into the CMOS platform to characterize ethanol sensing in this study.

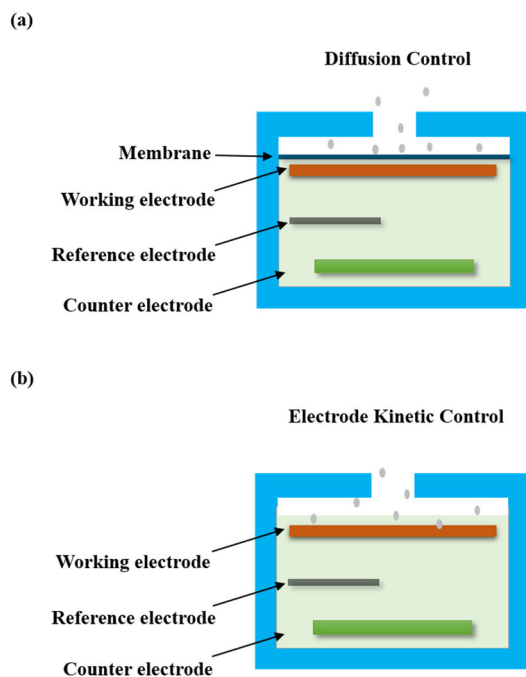


Fig. 1. Figure of two control mechanisms of amperometric gas sensors. (a) Diffusion control. (b) Electrode kinetic control.

In this regard, this study demonstrates the design of a micro amperometric gas sensor to detect ethanol gas at room temperature using the standard commercially available CMOS fabrication platform together with the post-CMOS micromachining processes. By leveraging the micromachining processes, the miniaturized amperometric sensor consists of a suspended electrode with a microhole structure as the working electrode, a fully anchored plate with a microhole structure as the counter electrode, and a microcavity as the electrolyte reservoir can be realized via the metal and oxide layers inherent in the CMOS processes. Such a suspended electrode is designed to shorten the diffusion time of gas to the electrode surface so as to improve the response time of the sensor. A microhole structure is designed to achieve a high electrode surface area to enhance the sensitivity of the sensor. In addition, the microcavity is also implemented to define a small electrolyte volume, enabling the real-time measurement of the sensor. The suspended electrode, the fully anchored electrode, and the microcavity structure can be integrated into the sensing chip through the processes. In order to detect the ethanol gas, a Ni-sensing film is deposited on the working electrode to induce ethanol oxidation. The following experiments demonstrate the feasibility of the presented sensors.

II. THEORY AND DESIGN CONCEPT

As shown in Fig. 1, based on sensor configurations, the amperometric gas sensor can be respectively operated in two different modes: the diffusion control mode and the electrode kinetic control mode [26]. For the case of diffusion control mode, as shown in Fig. 1(a), the membrane layer is exploited as the gas diffusion layer. Thus, the diffusion coefficient k of the gas to be detected can be controlled by the membrane layer,

with which the limiting current I_{limit} of the diffusion-controlled sensor is expressed by Fick's diffusion law as follows:

$$I_{\text{limit}} = k[C]_{\text{gas}} \quad (1)$$

where C is the gas concentration. In this design, the membrane could enhance the selectivity of the sensor and also prevent the leakage of electrolytes; however, the current signal will also be reduced with the existing membrane layer. According to (1), the output current is proportional to the gas diffusion coefficient k and the gas concentration C . On the other hand, in the case of electrode kinetic control mode, as displayed in Fig. 1(b), the gas molecules to be detected directly react with the working electrode. Thus, its limiting current, I_{limit} , is higher than that achieved from the diffusion control approach and can be expressed as follows:

$$I_{\text{limit}} = nFkACe^{\frac{\alpha nFE}{RT}} \quad (2)$$

where n represents the number of electrons per molecule reacting, F is the faraday constant, k represents the diffusion coefficient, A is the area of the electrode, C is the gas concentration, R is the gas constant, T is the Kelvin temperature, α is the transfer coefficient, and E is the overvoltage of the electrode reaction. According to (2), the output current can be improved by varying the working electrode area A , the gas diffusion coefficient k , and the gas concentration C . Note that, for both control modes, the gas diffusion plays a significant role in the sensor performance, as it can affect the response time [32], [33]. Thus, a suspended working electrode with a microhole structure is proposed in this study to enhance the gas diffusion and further improve the sensitivity and response time of the sensor.

This study presents the design and implementation of a micro amperometric gas sensor based on the standard commercial available CMOS platform together with the post-CMOS micromachining processes. Fig. 2 illustrates the schematic of the sensor design, in which the standard Taiwan Semiconductor Manufacturing Company, Taiwan (TSMC) 0.35 μm two polysilicon and four metal layers (2P4M) platform is adopted. The isometric drawing in Fig. 2(a) and the cross-section view in Fig. 2(b) indicate the proposed sensor consists of the suspended plate with a microhole structure as the working electrode and the fully anchored plate with a microhole structure as the counter electrode. These electrodes are formed by the metal layers of the CMOS processes, and an additional sensing layer is deposited on the working electrode to provide the gas catalytic properties. Moreover, the dielectric layer of the CMOS process is employed to enhance the stiffness of the suspended working electrode. The electrode with a microhole structure can increase its surface area, and hence, the sensitivity of the sensor can be enhanced. In addition, the suspended electrode is designed to reduce the gas diffusion time and further improve the response time of the sensor. A cavity is fabricated on the substrate surface that acts as an electrolyte reservoir. A small electrolyte volume reserved into the microcavity can also shorten the measurement time of the sensor [48]. The microcavity is filled with a Nafion dispersion activated in alkaline media,

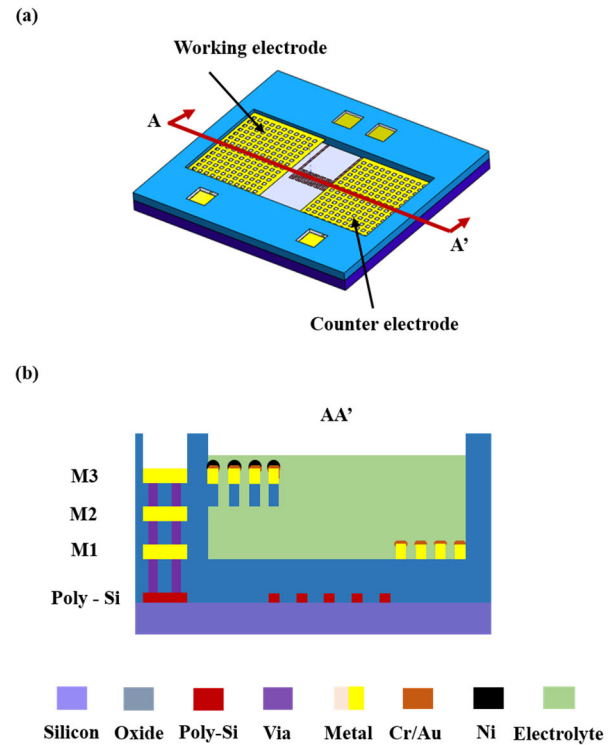


Fig. 2. Schematic illustrations of (a) proposed CMOS-MEMS amperometric gas sensor and (b) cross-section view of the amperometric gas sensor with electrolyte filling and Au/Ni sensing layers.

which transports the ion/water and supports the electrode structure. The micro heater is located at the center of the sensor structure. The cross-section view in Fig. 2(b) also indicates the metal (TiN/Al), dielectric (SiO_2), and polysilicon (Po-Si) layers are employed to implement the structure of the proposed amperometric gas sensor. In short, the first (M1) and the third (M3) metal layers are respectively used to fabricate the counter electrode and the working electrode. The cavity can be achieved after the etching of sacrificial metal and dielectric layers. In this study, the microhole size, the electrode area, the distance between electrodes, and the depth of the cavity are 2, 470×600 , 270, and 3.28 μm , respectively.

In application, the detection of ethanol is employed to demonstrate the feasibility of the presented CMOS-MEMS amperometric gas sensor. Fig. 3 exhibits the sensing mechanism of the proposed sensor to detect ethanol gas, and the Ni layer is used as the sensing material. When a voltage is applied to the working electrode, the Ni sensing layer is oxidized to higher oxidation states, such as $\text{NiO}/\text{NiOOH}/\text{Ni}(\text{OH})_2/\text{NiO}_2$, which releases an electron [49], [50]. The ethanol gas is oxidized on the sensing electrode and then releases more electrons. Thus, the ethanol gas concentration is determined by the output current of the sensing electrode.

III. FABRICATION AND RESULTS

The micro amperometric ethanol sensor is fabricated using the standard TSMC 0.35 μm 2P4M process first and followed up with the in-house post-CMOS micromachining process, as illustrated in Fig. 4. Fig. 4(a) shows the stacking and patterning of metal and dielectric layers on the CMOS chip

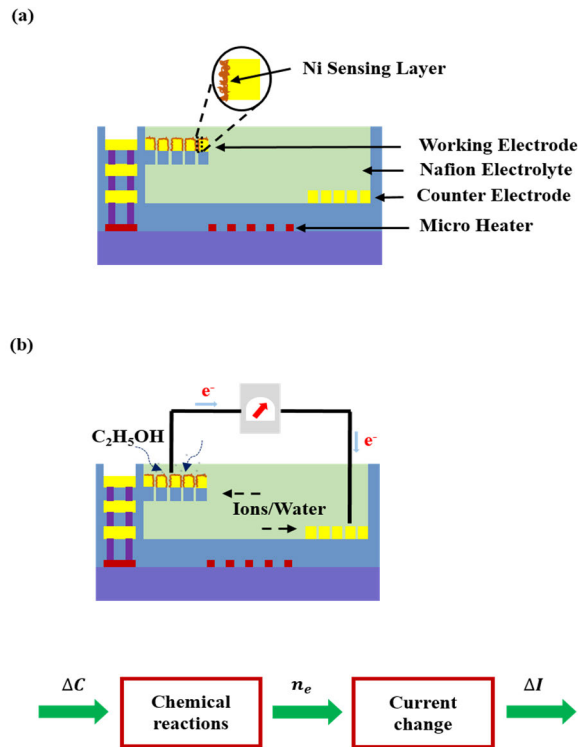


Fig. 3. Sensing schematic: (a) proposed CMOS-MEMS amperometric ethanol sensor and (b) flowing chart of ethanol sensor.

after the standard TSMC processes. After that, the H_2SO_4 and H_2O_2 solutions were used to etch away the metal layers (M1–M4 and tungsten vias layers), as depicted in Fig. 4(b). In this step, the metal layers acted as suspended working, and the anchored counter electrodes were protected by the dielectric layers. Moreover, microholes were formed on the suspended and anchored electrodes. It is noted that the electrolyte reservoir in this step had a depth D . As shown in Fig. 4(c), the protective oxide layer was removed by using reactive ion etching (RIE) to expose the metal electrodes and pads. The suspended metal electrode was supported by the dielectric layer underneath, which was not removed during the RIE. The Cr/Au layer was deposited on working and counter electrodes by E-gun (ULVAC FU-500CE), as depicted in Fig. 4(d). After that, the Ni sensing layer was deposited on working electrode at 200 °C by sputtering process (KD-THERMAL N-06G18). The shadow mask was employed to determine the selective deposition on the working electrode. Next, the pads on the sensing chip and printed circuit board (PCB) were connected by metal wires for electrical routings, as displayed in Fig. 4(e). The metal wires and pads were protected by epoxy. Finally, the electrolyte was dropped into the reservoir by pipette, as shown in Fig. 4(f), and the sensing chip was then ready for testing. The SEM and OM micrographs show more details about the microsensors that are prepared by TSMC after post-CMOS processes and after Au/Ni deposition. Micrographs in Fig. 5 display the typical fabrication results after the process in Fig. 4(c). As indicated in Fig. 5(a), the working electrode is positioned on the left-hand side, and the other side is the counter electrode. Zoom-in micrographs indicate that the M1 metal layer acts as the

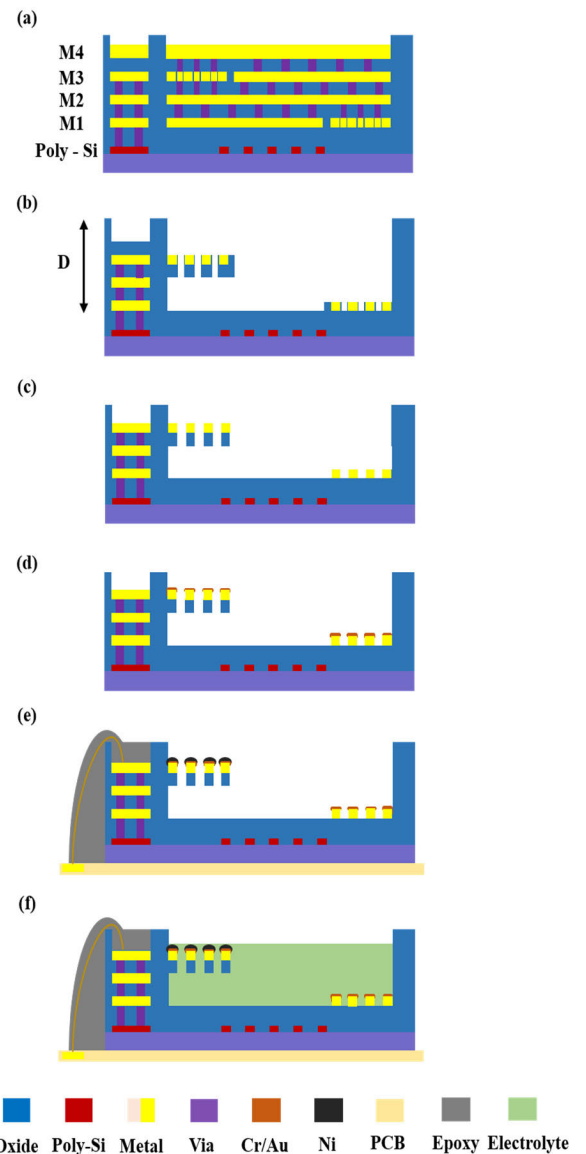


Fig. 4. Fabrication process steps: (a) prepared chip by the TSMC 2P4M CMOS process, (b) post-CMOS metal wet etching, (c) oxide etching, (d) Cr/Au deposition, (e) Ni deposition, and wire bonding and epoxy covering, and (f) electrolyte filling.

anchored counter electrode while the M3 metal layer serves as the suspended working electrode. Besides, as depicted in the top zoom-in micrograph, the microcavity with a depth of D is also observed. The zoom-in micrograph in Fig. 5(b) further displays the suspended working electrode with the metal (TiN and Al) and the oxide (SiO_2) layers. Besides, the zoom-in of the counter electrode shows the uniform microhole structure with 2 μm in hole size and 4 μm in hole distance, as displayed in Fig. 5(c). Micrographs in Fig. 6(a) display the fabrication results after the Cr/Au and Ni depositions in Fig. 4(d) and (e). The working electrode is partially covered with Cr/Au and Ni layers by using shadow masks. The left micrograph shows the misalignment of the shadow mask so that part of the TiN/Al layer was not covered with the Cr/Au film on the counter electrode. Micrographs in Fig. 6(b) show the fabricated chip after the process in Fig. 4(e). The chip contains sensor arrays

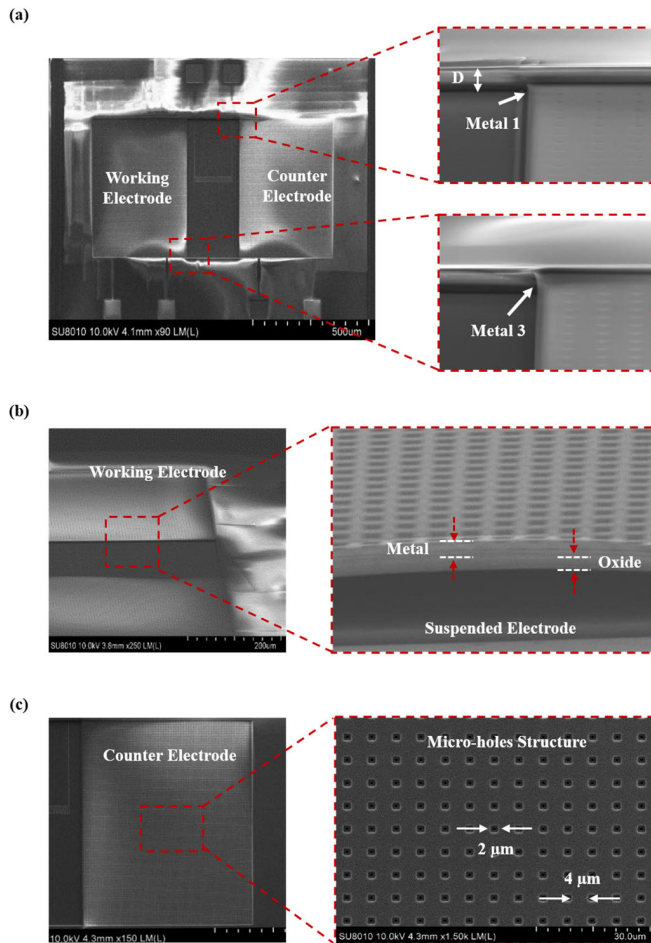


Fig. 5. SEM micrographs of typical fabricated amperometric sensor: (a) working and counter electrodes, and the zoom-in to show the related metal layers and the reservoir depth, (b) zoom-in of suspended working electrode to show metal/oxide layers, and (c) zoom-in of counter electrode to show a microhole structure.

(3 × 1) with 5.2 × 1.95 mm chip-out size and is wire bonded onto the PCB board as the device under test (DUT). All the bonded wires and chips are protected by epoxy. The zoom-in micrograph displays the micro amperometric sensor with Au and Ni layers.

IV. MEASUREMENTS AND DISCUSSIONS

The EC properties of the sensor are characterized by the experimental setup shown in Fig. 7. The potentiostat system (AUTOLAB PGSTAT302N) is used to supply the scanned voltage and frequency to the sensors and measure the output current and impedance (real/imaginary parts). Thus, the cyclic voltammetry (CV) and EC spectroscopy impedance (EIS) characteristics of the sensor are measured. The working terminal (WT) of the potentiostat connects to the working electrode of sensors, and the reference (RT) and counter (CT) terminals of potentiostat are connected to the counter electrode of sensors. In this experiment, the DUT in Fig. 6(b) was measured in both ethanol and air. The mixtures of ethanol (99% Aldrich), Nafion (Dispersion D520), and 0.01M KOH were prepared in various concentrations (10, 50, 100, and 200 ppm). The measurement setup in Fig. 7 is also employed to demonstrate the gas-sensing properties of the presented

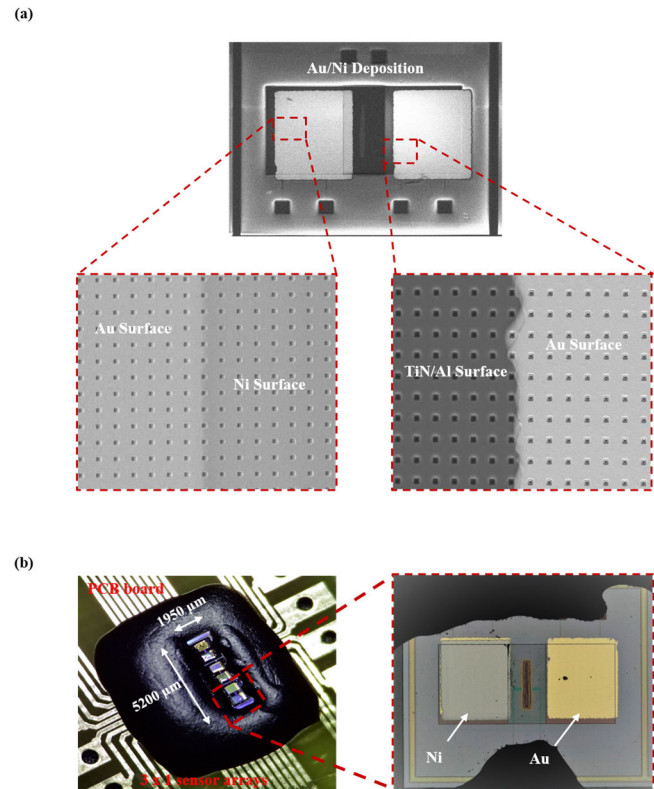


Fig. 6. Micrographs of typical fabricated amperometric sensor: (a) after the deposition of Au and Ni layers and (b) amperometric sensor array chip wire-bonded on the PCB.

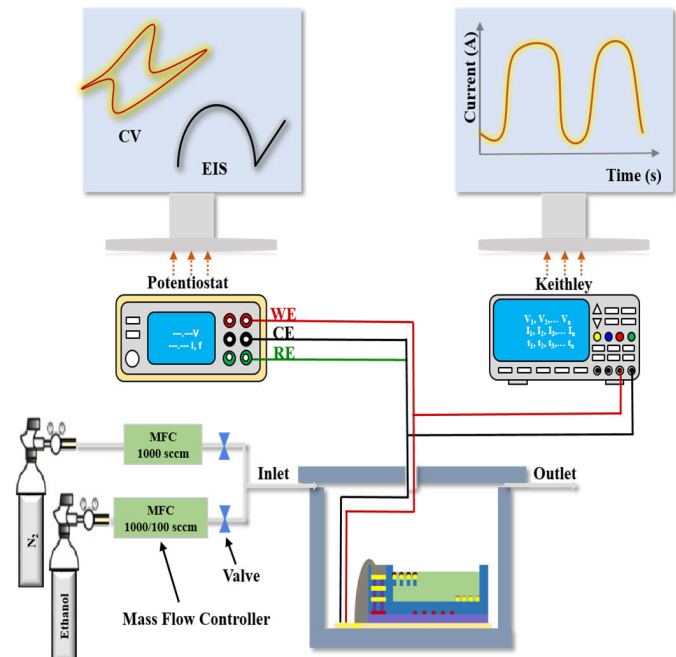


Fig. 7. Schematic of the measurement set-up: test of EC properties and the ethanol sensing characteristics.

sensors. The target gas and nitrogen are controlled by the mass-flow-controller (MFC) in order to achieve the desired gas concentration in the test chamber. The source meter (Keithley 4200) is used to supply the operated voltage to the sensor, and sensing signals are recorded by the computer.

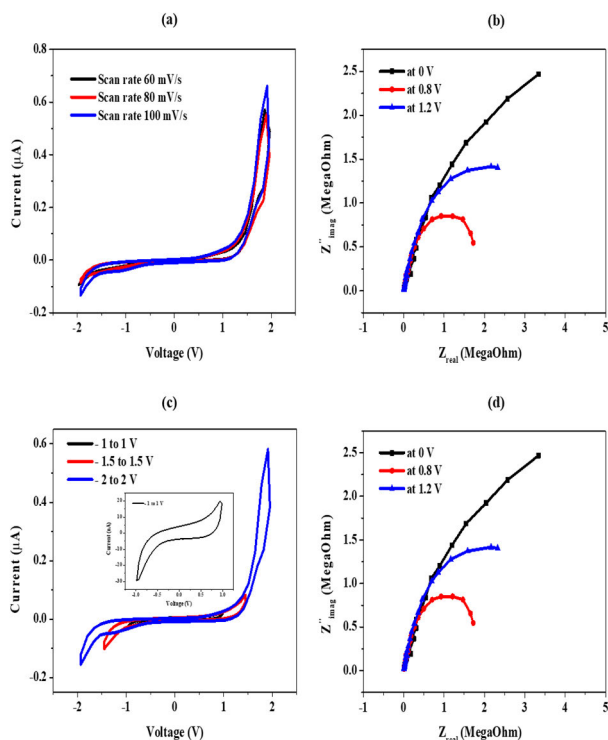


Fig. 8. CV and EC impedance spectroscopy measurements of amperometric sensors based on TiN/Al/Au electrode at: (a) scan rates of 60, 80, and 100 mV/s, (b) scan rate of 100 mV/s for 5 cycles, (c) 100 mV/s in different potential windows, and (d) applied voltages of 0, 0.8, and 1.2 V.

First, this study evaluates the characteristics of the proposed sensors with TiN/Al/Au working electrodes. To avoid the destruction of an electrode, reasonable values of scan rate are chosen in EC measurements. Fig. 8(a) shows the measured CV of the sensor, and the curves show linear characteristics at three scan rates of 60, 80, and 100 mV/s. As depicted in Fig. 8(b), such a characteristic is preserved in five cycles at 100 mV/s to show the repeatability of the sensors. To characterize the oxidation/reduction regions, the sensors are scanned at various potential windows, as shown in Fig. 8(c). The results show that the oxidation regions can be originated at nearly 0.7–0.8 and 1.6 V. These regions can be attributed to the oxidation of TiN/Au to form Ti-OH groups [51], [52], and TiN/Al to form the $\text{TiO}_2/\text{Al}_2\text{O}_3$. Moreover, Fig. 8(d) exhibits the EIS characteristics measured at three applying voltages 0, 0.8, and 1.2 V. The highest electron/charge transfer is found at 0.8 V to show the oxidation of TiN/Au. The CV and EIS characteristics of the sensors with TiN/Al/Au working electrodes are also investigated in the presence of ethanol, as shown in Fig. 9(a). Measurements reveal that the output current is decreased with the increase in ethanol concentration. Moreover, the inset EIS measurement in Fig. 9(a) shows that the impedance of the sensor is expanded in the presence of ethanol compared to that in the air. The current dropping and impedance expansion are caused by the formation of an oxide layer and the lower conductivity of the electrolyte. The gas-sensing characteristic of the sensor with TiN/Al/Au working electrode is demonstrated to 1000 ppm ethanol at room temperature, as displayed in Fig. 9(b). The output current will eventually drop to zero, which witnesses the formation of thin

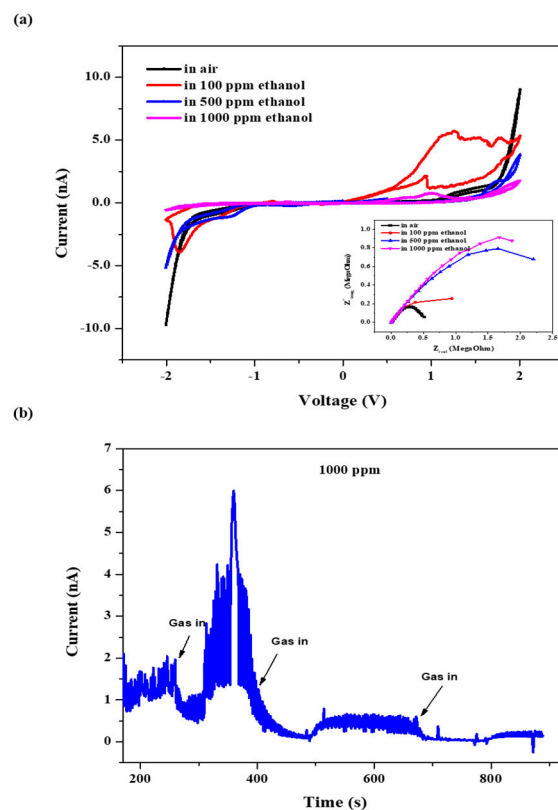


Fig. 9. Measurements of amperometric sensors based on TiN/Al/Au electrode in air and in ethanol: (a) CV and the inset of (a) EC impedance spectroscopy and (b) in 1000 ppm ethanol at room temperature.

oxide layers on the electrode surface. Thus, the sensor with TiN/Al/Au working electrode is insensitive to ethanol gas.

For comparison, the proposed sensors with TiN/Al/Au/Ni working electrodes are also tested in this study. Fig. 10 shows the CV and EIS characteristics of the sensor in air and different ethanol concentrations (10, 50, 100, and 200 ppm). As depicted in Fig. 10(a), the two main oxidation peaks are found around 0.35 V (peak A) and 0.65 V (peak B) in the forward scan, which refers to the mechanism of Ni oxidation at 50 mV/s. In the presence of ethanol, the two oxidation peaks are shifted to 0.4–0.5 V (peak A') and 0.75–0.9 V (peak B'). This can be ascribed to the complete/incomplete oxidation of ethanol on the electrode surface. The output currents are increased with the increase in ethanol concentrations from 10 to 100 ppm; however, the current is slightly decreased as ethanol concentration reaches 200 ppm. It can be due to the restriction of ethanol diffusion to the sensing electrode through an intermediated product. The EIS measurements in inset Fig. 10(a) also demonstrate that the sensor impedance decreases with the increase of ethanol concentration. The lowest impedance is found at 100 ppm ethanol and 0.8 V applied voltage. These results agree well with the CV measurements. Thus, the proposed sensors with TiN/Al/Au/Ni working electrodes could detect ethanol in the range of ppm. The gas-sensing characteristic of the sensor with TiN/Al/Au/Ni working electrodes to 1000 ppm ethanol at 0.8 V is shown in Fig. 10(b). The output current increases upon ethanol exposure and the sensitivity is estimated at 0.011 nA/ppm. Because of the limitation of MFC, the smallest

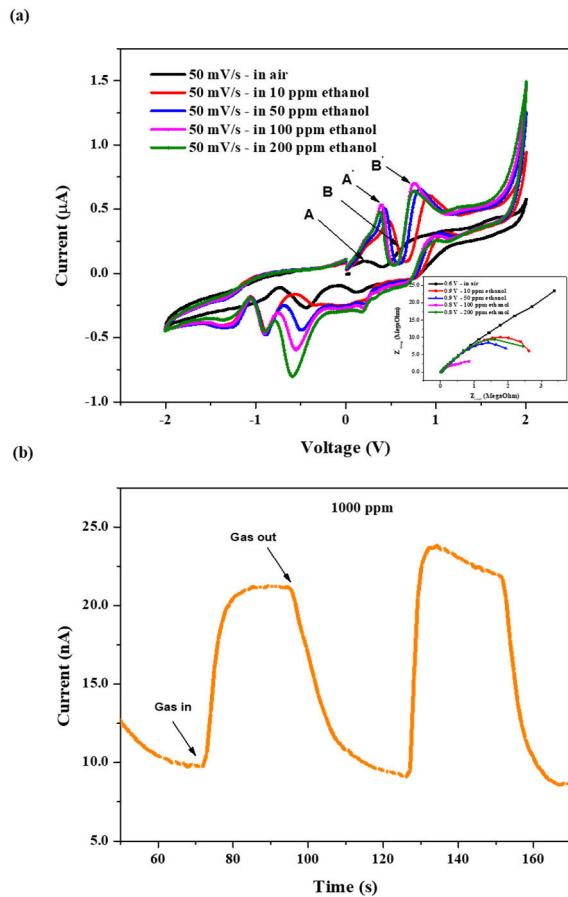


Fig. 10. Measurements of amperometric sensors based on TiN/Al/Au/Ni electrode in air and in ethanol: (a) CV and the inset of (a) EC impedance spectroscopy and (b) in 1000 ppm ethanol at room temperature.

gas concentration this study can properly control is 20 ppm. The sensor is measured in large (50–1000 ppm) and small (20–150 ppm) ranges of ethanol concentrations at room temperature, as shown in Fig. 11(a). The results indicate that the output current increases with the rise of ethanol concentration. Fig. 11(b) further depicts the output current versus ethanol gas concentration, and hence, the sensitivity and linearity of the proposed sensor are determined. For a large range (50–1000 ppm) of ethanol concentration, the sensitivity and linearity of the proposed sensor are 0.01 nA/ppm and 0.955, respectively. For a small range (20–150 ppm) of ethanol concentration, the sensitivity and linearity of the sensor become 0.08 nA/ppm and 0.959, respectively. The different sensitivity may be due to the rate of electrode reaction/gas diffusion [52]. Thus, the limit of detection (LOD) of the sensor is <20 ppm within the ethanol concentration range of 20–150 ppm, as indicated in the inset of Fig. 11(b). In addition, the measurements in Fig. 11(c) depict that the sensor has the response time of nearly 6 s in 500 ppm ethanol at room temperature. The good sensitivity and fast response time of the presented sensor are attributed to the suspended electrode with a microhole structure. Table I shows the sensing characteristics of the presented sensor in comparison with other works at the chip scale. Note that these references focus

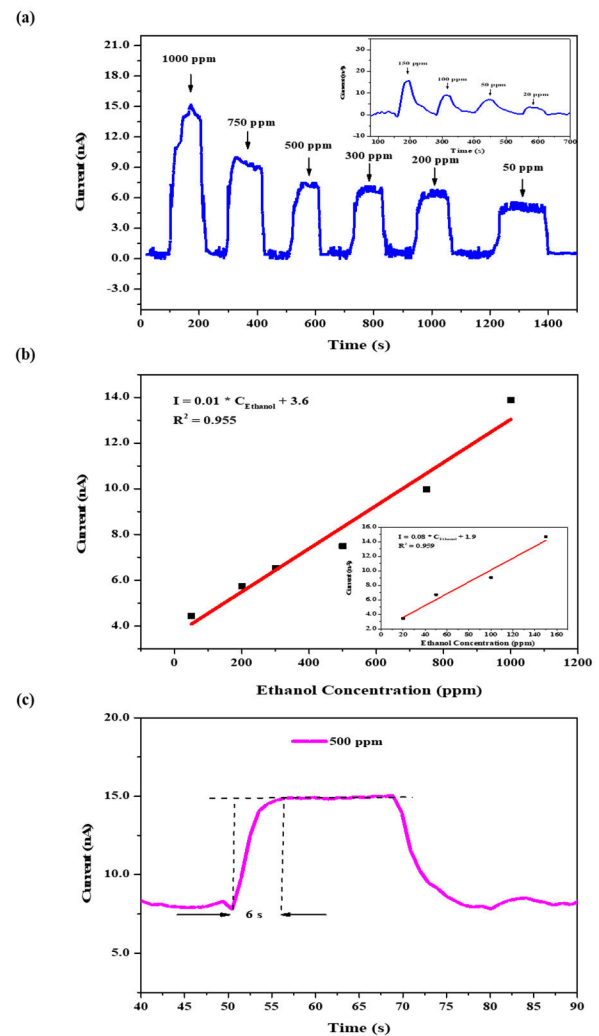


Fig. 11. Gas sensing characteristics of the presented amperometric sensor based on the TiN/Al/Au/Ni electrode: (a) in ethanol concentrations of 1000, 750, 500, 300, 200, and 50 ppm, (b) sensitivity of sensor, and (c) response time of sensor at 500 ppm ethanol. The inset of (a) sensor properties and (b) sensitivity in ethanol concentrations of 150, 100, 50, and 20 ppm.

on sensing materials to achieve high sensitivity rather than sensor design.

This study also evaluates the selectivity of the presented sensor with the presence of 150 ppm ethanol, 150 ppm acetone, 1000 ppm NO₂, 5 ppm HCHO, and 50 ppm NH₃ gases. Note the commercially available gases with a specific concentration were respectively prepared in containers to input into the chamber with a sensor to ensure the gas concentration during testing. Measurements in Fig. 12(a) reveal that the sensor has a higher output current for ethanol, as compared with that for acetone of the same concentration. Moreover, the output current of sensor for the ethanol is near sevenfold higher than that for HCHO and NH₃ gases. The sensor has also responded to NO₂ at high concentrations. The acetone and NO₂ sensing characteristics can be deduced from a thin native NiO film on the electrode surface [53], [54]. Fig. 12(b) shows the sensor responses (at 150 ppm ethanol) varying with the relative humidity (RH) (respectively at 42%, 54%, 65%, and 78% RH). The variation may be due to the change in

TABLE I
COMPARISONS OF THE ETHANOL SENSING PROPERTIES WITH OTHER WORKS (CHIP-SCALE)

	Reference [55]	Reference [56]	Reference [57]	This study
Type	MOS	MOS	MOS	Amperometric
Sensing materials	Pd/SnO ₂ :NiO	In ₂ O ₃	ZnO	Ni/Au/Al/TiN
Sensing area	150 × 150 μm ²	x	2000 × 2000 μm ²	600 × 470 μm ²
Chip size	5 × 5 mm ²	x	5 × 5 mm ²	1.36 × 0.75 mm ²
Target gases	Ethanol	Ethanol	Ethanol	Ethanol
Sensitivity	0.18	0.0026	0.0075	0.01
Response time	x	10 s	> 150 s	6 s
Limit of detection (LOD)	< 5 ppm	20 ppm	x	< 20 ppm
Operating temperature	325 ~ 400 °C	Room temperature	100 °C	Room temperature

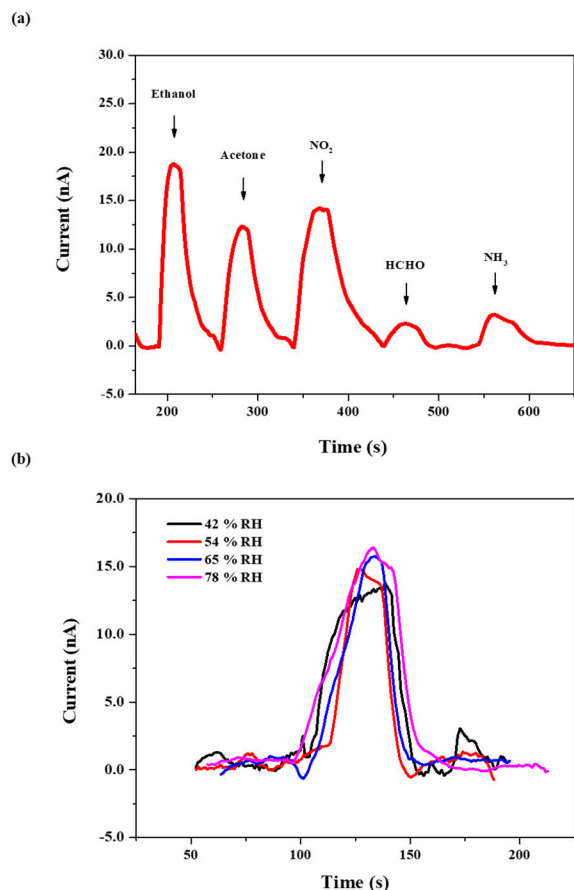


Fig. 12. Measurements of amperometric sensor: (a) selectivity of sensor in 150 ppm ethanol, 150 ppm acetone, 1000 ppm NO₂, 5 ppm HCHO, and 50 ppm NH₃ gases at room temperature and (b) dependence of sensitivity on RH at 150 ppm ethanol.

electrolyte conductivity. The higher humidity can lead to a larger conductivity, resulting in an increase of output current. It is worth noting that the presented gas sensor exhibits much smaller sensitivity variation in high humidity environments compared to the MOS type counterpart [10].

V. CONCLUSION

This study presents a miniaturized amperometric gas sensor for rapid measurement of ethanol at room temperature. The micro-amperometric ethanol sensing chip is first fabricated using the TSMC 0.35 μm 2P4M standard CMOS process. The suspended microhole working electrode, the fully anchored microhole counter electrode, and the electrolyte reservoir are

defined via post-CMOS process. The Cr/Au layer is deposited on the electrodes to limit the Al corrosion, and Ni-sensing layer is sputtered on the working electrode to achieve ethanol sensing. The sensitivity and response time of the sensors are significantly improved by using the suspended electrode with a microhole structure. A small electrolyte volume defined by microcavity can also contribute to the short measurement time. Measurements show that the sensitivity and response time of sensors are, respectively, 0.01 nA/ppm and 6 s at room temperature. In addition, the sensor also demonstrates its selectivity among the ethanol, acetone, NO₂, HCHO, and NH₃ gases. In summary, the CMOS-MEMS amperometric sensor shows good sensitivity, fast response time, and good selectivity to ethanol gas at atmospheric conditions.

ACKNOWLEDGMENT

The authors would like to appreciate the Taiwan Semiconductor Manufacturing Company (TSMC) and the Taiwan Semiconductor Research Institute (TSRI) for the supporting of CMOS chip manufacturing. They would also like to appreciate the Center for Nanotechnology, Materials Science and Microsystems (CNMM) of National Tsing Hua University for providing the tools in the processes. Finally, our warmest thanks to the lab members of Micro Device Laboratory, Nanoscience and Nanodevices Laboratory from NTHU and the PixArt imaging Inc., Taiwan for their invaluable assistance.

REFERENCES

- [1] T. Chen, T. Liu, T. Li, H. Zhao, and Q. Chen, "Exhaled breath analysis in disease detection," *Clinica Chim. Acta*, vol. 515, pp. 61–72, Apr. 2021.
- [2] S. Das and M. Pal, "Review—Non-invasive monitoring of human health by exhaled breath analysis: A comprehensive review," *J. Electrochem. Soc.*, vol. 167, no. 3, Jan. 2020, Art. no. 037562.
- [3] S. Mojumder, T. Das, S. Das, N. Chakraborty, D. Saha, and M. Pal, "Y and Al co-doped ZnO-nanopowder based ultrasensitive trace ethanol sensor: A potential breath analyzer for fatty liver disease and drunken driving detection," *Sens. Actuators B, Chem.*, vol. 372, Dec. 2022, Art. no. 132611.
- [4] H.-L. Yu et al., "Fabrication of single crystalline WO₃ nano-belts based photoelectric gas sensor for detection of high concentration ethanol gas at room temperature," *Sens. Actuators A, Phys.*, vol. 303, Mar. 2020, Art. no. 111865.
- [5] P. F. Cao et al., "Preparation and characterization of a novel ethanol gas sensor based on FeYO₃ microspheres by using orange peels as bio-templates," *Vacuum*, vol. 177, Jul. 2020, Art. no. 109359.
- [6] J. Razumien et al., "Amperometric detection of glucose and ethanol in beverages using flow cell and immobilised on screen-printed carbon electrode PQQ-dependent glucose or alcohol dehydrogenases," *Sens. Actuators B, Chem.*, vol. 78, nos. 1–3, pp. 243–248, Aug. 2001.

- [7] B. Sharma, K. Karuppasamy, D. Vikraman, E.-B. Jo, P. Sivakumar, and H.-S. Kim, "Porous, 3D-hierarchical α -NiMoO₄ rectangular nanosheets for selective conductometric ethanol gas sensors," *Sens. Actuators B, Chem.*, vol. 347, Nov. 2021, Art. no. 130615.
- [8] C. Patel et al., "S, N co-doped carbon dot-functionalized WO₃ nanostructures for NO₂ and H₂S detection," *ACS Appl. Nano Mater.*, vol. 5, no. 2, pp. 2492–2500, Feb. 2022.
- [9] C. Patel et al., "Large and uniform single crystals of MoS₂ monolayers for ppb-level NO₂ sensing," *ACS Appl. Nano Mater.*, vol. 5, no. 7, pp. 9415–9426, Jul. 2022.
- [10] L. Xu et al., "Micro/nano gas sensors: A new strategy towards in-situ wafer-level fabrication of high-performance gas sensing chips," *Sci. Rep.*, vol. 5, no. 1, p. 10507, May 2015.
- [11] J. Wang et al., "Gas detection microsystem with MEMS gas sensor and integrated circuit," *IEEE Sensors J.*, vol. 18, no. 16, pp. 6765–6773, Aug. 2018.
- [12] J. C. Belmonte et al., "Micromachined twin gas sensor for CO and O₂ quantification based on catalytically modified nano-SnO₂," *Sens. Actuators B, Chem.*, vol. 114, no. 2, pp. 881–892, Apr. 2006.
- [13] A. Adami et al., "A WO₃-based gas sensor array with linear temperature gradient for wine quality monitoring," *Sens. Actuators B, Chem.*, vol. 117, no. 1, pp. 115–122, Sep. 2006.
- [14] K. K. Park et al., "Capacitive micromachined ultrasonic transducer (CMUT) as a chemical sensor for DMMP detection," *Sens. Actuators B, Chem.*, vol. 160, no. 1, pp. 1120–1127, Dec. 2011.
- [15] P. Mohankumar, J. Ajayan, R. Yasodharan, P. Devendran, and R. Sambasivam, "A review of micromachined sensors for automotive applications," *Measurement*, vol. 140, pp. 305–322, Jul. 2019.
- [16] K. D. Mitzner, J. Sternhagen, and D. W. Galipeau, "Development of a micromachined hazardous gas sensor array," *Sens. Actuators B, Chem.*, vol. 93, nos. 1–3, pp. 92–99, Aug. 2003.
- [17] A. A. Vasiliev and V. V. Malyshev, "Sensors for the ultra-fast monitoring of explosive gas concentrations," *Sens. Actuators B, Chem.*, vol. 189, pp. 260–267, Dec. 2013.
- [18] L. Francioso et al., "Linear temperature microhotplate gas sensor array for automotive cabin air quality monitoring," *Sens. Actuators B, Chem.*, vol. 134, no. 2, pp. 660–665, Sep. 2008.
- [19] T. Goto, T. Itoh, T. Akamatsu, Y. Sasaki, K. Sato, and W. Shin, "Heat transfer control of micro-thermoelectric gas sensor for breath gas monitoring," *Sens. Actuators B, Chem.*, vol. 249, pp. 571–580, Oct. 2017.
- [20] A. Bagolini et al., "Development of MEMS MOS gas sensors with CMOS compatible PECVD inter-metal passivation," *Sens. Actuators B, Chem.*, vol. 292, pp. 225–232, Aug. 2019.
- [21] C. Lim, W. Wang, S. Yang, and K. Lee, "Development of SAW-based multi-gas sensor for simultaneous detection of CO₂ and NO₂," *Sens. Actuators B, Chem.*, vol. 154, no. 1, pp. 9–16, May 2011.
- [22] S. Khan, S. Le Calvé, and D. Newport, "A review of optical interferometry techniques for VOC detection," *Sens. Actuators A, Phys.*, vol. 302, Feb. 2020, Art. no. 111782.
- [23] J. Lee et al., "Low power consumption solid electrochemical-type micro CO₂ gas sensor," *Sens. Actuators B, Chem.*, vol. 248, pp. 957–960, Sep. 2017.
- [24] J.-H. Han, S. Kim, J. Choi, S. Kang, Y. K. Pak, and J. J. Pak, "Development of multi-well-based electrochemical dissolved oxygen sensor array," *Sens. Actuators B, Chem.*, vol. 306, Mar. 2020, Art. no. 127465.
- [25] Y. Chao et al., "Amperometric sensor for selective and stable hydrogen measurement," *Sens. Actuators B, Chem.*, vol. 106, no. 2, pp. 784–790, 2005.
- [26] J. R. Stetter and J. Li, "Amperometric gas sensors a review," *Chem. Rev.*, vol. 108, no. 2, pp. 352–366, 2008.
- [27] G. Hussain, M. Ge, C. Zhao, and D. S. Silvester, "Fast responding hydrogen gas sensors using platinum nanoparticle modified microchannels and ionic liquids," *Analytica Chim. Acta*, vol. 1072, pp. 35–45, Sep. 2019.
- [28] H. K. Gatty, G. Stemme, and N. Roxhed, "A wafer-level liquid cavity integrated amperometric gas sensor with ppb-level nitric oxide gas sensitivity," *J. Micromech. Microeng.*, vol. 25, no. 10, Oct. 2015, Art. no. 105013.
- [29] S. Petralia et al., "Miniaturized and multi-purpose electrochemical sensing device based on thin Ni oxides," *Sens. Actuators B, Chem.*, vol. 263, pp. 10–19, Jun. 2018.
- [30] H. Wan, H. Yin, and A. J. Mason, "Rapid measurement of room temperature ionic liquid electrochemical gas sensor using transient double potential amperometry," *Sens. Actuators B, Chem.*, vol. 242, pp. 658–666, Apr. 2017.
- [31] P. Jacquinet, A. W. E. Hodgson, and P. C. Hauser, "Amperometric detection of NO and NO₂ in the ppb range with solid-polymer electrolyte membrane supported noble metal electrodes," *Analytica Chim. Acta*, vol. 443, no. 1, pp. 53–61, Sep. 2001.
- [32] D. S. Silvester, "New innovations in ionic liquid-based miniaturised amperometric gas sensors," *Current Opinion Electrochemistry*, vol. 15, pp. 7–17, Jun. 2019.
- [33] J. F. M. Oudenhoven, W. Knobben, and R. Van Schaijk, "Electrochemical detection of ammonia using a thin ionic liquid film as the electrolyte," *Proc. Eng.*, vol. 120, pp. 983–986, Sep. 2015.
- [34] P. Gross, T. Larsen, F. Loizeau, T. Jaramillo, D. Spitzer, and B. Pruitt, "Microfabricated electrochemical gas sensor," *Micro Nano Lett.*, vol. 11, no. 12, pp. 798–802, Dec. 2016.
- [35] Y. Guan et al., "Highly sensitive amperometric nafion-based CO sensor using Pt/C electrodes with different kinds of carbon materials," *Sens. Actuators B, Chem.*, vol. 239, pp. 696–703, Feb. 2017.
- [36] H. K. Gatty, S. Leijonmarck, M. Antelius, G. Stemme, and N. Roxhed, "An amperometric nitric oxide sensor with fast response and ppb-level concentration detection relevant to asthma monitoring," *Sens. Actuators B, Chem.*, vol. 209, pp. 639–644, Mar. 2015.
- [37] H. Wan, H. Yin, L. Lin, X. Zeng, and A. J. Mason, "Miniaturized planar room temperature ionic liquid electrochemical gas sensor for rapid multiple gas pollutants monitoring," *Sens. Actuators B, Chem.*, vol. 255, pp. 638–646, Feb. 2018.
- [38] H. Yin, X. Mu, H. Li, X. Liu, and A. J. Mason, "CMOS monolithic electrochemical gas sensor microsystem using room temperature ionic liquid," *IEEE Sensors J.*, vol. 18, no. 19, pp. 7899–7906, Oct. 2018.
- [39] Y.-C. Lee et al., "CMOS-MEMS technologies for the applications of environment sensors and environment sensing hubs," *J. Micromech. Microeng.*, vol. 31, no. 7, Jul. 2021, Art. no. 074004.
- [40] J. T. S. Allan, H. L. Geoffrey, and E. B. Easton, "The effect of the gas diffusion layer on the performance of fuel cell catalyst layers in ethanol sensors," *Sens. Actuators B, Chem.*, vol. 254, pp. 120–132, Jan. 2018.
- [41] R. A. Gonçalves, M. R. Baldan, E. G. Ciapina, and O. M. Berengue, "Nanostructured Pd/Sb₂O₃: A new and promising fuel cell electrocatalyst and non-enzymatic amperometric sensor for ethanol," *Appl. Surf. Sci.*, vol. 491, pp. 9–15, Oct. 2019.
- [42] Y. Oh, S.-K. Kim, D.-H. Peck, J.-S. Jang, J. Kim, and D.-H. Jung, "Improved performance using tungsten carbide/carbon nanofiber based anode catalysts for alkaline direct ethanol fuel cells," *Int. J. Hydrogen Energy*, vol. 39, no. 28, pp. 15907–15912, Sep. 2014.
- [43] M. T. Pham, M. F. Maitz, E. Richter, H. Reuther, F. Prokert, and A. Mucklich, "Electrochemical behaviour of nickel surface-alloyed with copper and titanium," *J. Electroanal. Chem.*, vol. 572, no. 1, pp. 185–193, Oct. 2004.
- [44] X.-C. Zhou et al., "Single-crystalline ultrathin nanofilms of Ni aerogel with Ni(OH)₂ hybrid nanoparticles towards enhanced catalytic performance for ethanol electro-oxidation," *Appl. Surf. Sci.*, vol. 492, pp. 756–764, Oct. 2019.
- [45] Z. Li and J. Yi, "Enhanced ethanol sensing of Ni-doped SnO₂ hollow spheres synthesized by a one-pot hydrothermal method," *Sens. Actuators B, Chem.*, vol. 243, pp. 96–103, May 2017.
- [46] J. Bai et al., "Role of nickel dopant on gas response and selectivity of electrospun indium oxide nanotubes," *J. Colloid Interface Sci.*, vol. 560, pp. 447–457, Feb. 2020.
- [47] S. Mehmood et al., "MoO₂-Ni-graphene ternary nanocomposite for a high—Performance room-temperature ethanol gas sensor," *Appl. Surf. Sci.*, vol. 554, Jul. 2021, Art. no. 149595.
- [48] K. Ishizu et al., "Carbon dioxide gas sensor with ionic gel," in *Proc. 17th Int. Conf. Solid-State Sensors, Actuat. Microsyst.*, 2013, pp. 1633–1636.
- [49] A. F. B. Barbosa, V. L. Oliveira, J. van Drunen, and G. Tremiliosi-Filho, "Ethanol electro-oxidation reaction using a polycrystalline nickel electrode in alkaline media: Temperature influence and reaction mechanism," *J. Electroanal. Chem.*, vol. 746, pp. 31–38, Jun. 2015.
- [50] J.-J. Huang, W.-S. Hwang, Y.-C. Weng, and T.-C. Chou, "Electrochemistry of ethanol oxidation on Ni-Pt alloy electrodes in KOH solutions," *Mater. Trans.*, vol. 50, no. 5, pp. 1139–1147, 2009.
- [51] M. M. O. Thotiyil, T. R. Kumar, and S. Sampath, "Pd supported on titanium nitride for efficient ethanol oxidation," *J. Phys. Chem. C*, vol. 114, no. 41, pp. 17934–17941, Oct. 2010.

- [52] D. Meng et al., "Platinum decorated mesoporous titanium nitride for fuel-cell type methanol gas sensor," *Sens. Actuators B, Chem.*, vol. 308, Apr. 2020, Art. no. 127713.
- [53] I. Hotovy et al., "Preparation and gas-sensing properties of very thin sputtered NiO films," *J. Electr. Eng.*, vol. 72, no. 1, pp. 61–65, Feb. 2021.
- [54] I. Hotovy, V. Rehacek, P. Siciliano, S. Capone, and L. Spiess, "Sensing characteristics of NiO thin films as NO₂ gas sensor," *Thin Solid Films*, vol. 418, no. 1, pp. 9–15, Oct. 2002.
- [55] Y. Wang, W. G. Tong, and N. Han, "Co-sputtered Pd/SnO₂:NiO heterostructured sensing films for MEMS-based ethanol sensors," *Mater. Lett.*, vol. 273, Aug. 2020, Art. no. 127924.
- [56] D. N. Son et al., "A novel design and fabrication of self-heated In₂O₃ nanowire gas sensor on glass for ethanol detection," *Sens. Actuators A, Phys.*, vol. 345, Oct. 2022, Art. no. 113769.
- [57] H. J. Pandya, S. Chandra, and A. L. Vyas, "Integration of ZnO nanostructures with MEMS for ethanol sensor," *Sens. Actuators B, Chem.*, vol. 161, no. 1, pp. 923–928, Jan. 2012.



Do Thi Thu was born in Hai Duong, Vietnam. She received the B.S. degree in quantum optics from the University of Education, Vietnam National University, Ha Noi, Vietnam, in 2010, the M.S. degree in materials and nanodevices from the University of Engineering and Technologies, Vietnam National University, in 2014. She is currently pursuing the Ph.D. degree with the Institute of Nanoengineering and Microsystems, National Tsing Hua University, Hsinchu, Taiwan.

Her current research interests are design and implementation of a chip-scale gas sensors via CMOS-MEMS process.



Zong-Han Liu was born in Chaiyi, Taiwan. He received the B.S. degree from the Department of Mechatronics Engineering, National Changhua University of Education, Changhua City, Taiwan, in 2012, and the M.S. degree from the Department of Power Mechanical Engineering, National Tsing Hua University, Hsinchu, Taiwan, in 2021.



Ya-Chu Lee was born in Yunlin, Taiwan. She received the B.S. and M.S. degrees from the Department of Automatic Control Engineering, Feng Chia University, Taichung, Taiwan, in 2012 and 2014, respectively, and the Ph.D. degree from the Department of Power Mechanical Engineering, National Tsing Hua University, Hsinchu, Taiwan, in 2022.

Her main interests include the design and implementation of the CMOS-MEMS gas sensor and integration of environmental sensors.



Tzu-Wen Kuo is currently pursuing the Ph.D. degree with the Department of Materials Science and Engineering, National Tsing Hua University, Hsinchu, Taiwan.

She joined the Master program at the Institute of NanoEngineering and MicroSystems, National Tsing Hua University, in 2012. She has then transferred to the Ph.D. program with the Department of Materials Science and Engineering, National Tsing Hua University, in 2020.



Wei-Lun Sung received the Ph.D. degree from National Tsing Hua University, Hsinchu, Taiwan, in 2016.

He currently works as a Section Manager with PixArt Imaging Inc., Hsinchu. His current research interests include far infrared sensor for applications, optical sensing, and MEMS manufacturing.



Yen-Chang Chu received the B.S. and Ph.D. degrees from the Department of Materials Science and Engineering, National Tsing Hua University, Hsinchu, Taiwan, in 2001 and 2008, respectively.

He is currently a Section Manager in PixArt Imaging Inc., Hsinchu. His research interests include CMOS image sensor, application of optical sensor, finite element analysis, semiconductor process, and material science.



Yu-Lun Chueh (Senior Member, IEEE) was born in Yilan, Taiwan. He received the Ph.D. degree from the Department of Materials Science and Engineering, National Tsing Hua University, Hsinchu, Taiwan, in 2006.

He worked as a Postdoctoral Researcher at the Electrical Engineering and Computer Sciences, University of California, Berkeley, CA, USA, in 2008. He is now as a Distinguished Professor at the Department of Materials Science and Engineering, National Tsing Hua University.

His research interests include development of various method to synthesize different graphene/2-D material, low power resistive random access memory, growth of low dimensional materials and its possible functional applications, and development of Cu(In, Ga)Se₂ solar cell and its investigation on light harvesting behaviors.

Dr. Chueh is now the Chief Editor of *Nanoscale Research Letters*, an Associate Editor of *Nanoscience and Nanotechnology Letters*, and the Editorial Board of *Journal of nanomaterials and Scientific Reports*.



Weileun Fang (Fellow, IEEE) was born in Taipei, Taiwan. He received the Ph.D. degree from Carnegie Mellon University, Pittsburgh, PA, USA, in 1995.

His doctoral research focused on the determining of the mechanical properties of thin films using micromachined structures. In 1995, he worked as a Postdoctoral Researcher at Synchrotron Radiation Research Center, Hsinchu, Taiwan. He joined the Power Mechanical Engineering Department at the National Tsing Hua University, Hsinchu, in 1996, where he is now the Chair Professor as well as a Faculty of NEMS Institute. In 1999, he was with Prof. Y.-C. Tai at California Institute Technology, Pasadena, CA, USA, as a Visiting Associate. He recognize his contribution in MEMS area. His research interests include MEMS with emphasis on micro fabrication/packaging technologies, CMOS MEMS, CNT MEMS, micro optical systems, micro sensors and actuators, and characterization of thin film mechanical properties.

Dr. Fang served as a member of International Steering Committee (ISC) of Transducers in 2009–2017 and the ISC Chair in 2017–2019. He also served as the General Chair of Transducers Conference, in 2017. He was the Technical Program Committee Member of IEEE Micro-Electromechanical Systems and Engineering, Procurement, and Construction of Transducers for many years, and the Program Chair of IEEE Sensors Conference in 2012. He served as the Chief Delegate of Taiwan for the World Micromachine Summit (MMS), from 2008 to 2012, and the General Chair of MMS, in 2012. He has close collaboration with MEMS industries and is now the VP of MEMS and Sensors Committee of SEMI Taiwan. He is now the Chief Editor of *Journal of Medical Microbiology*, an Associate Editor of IEEE SENSORS JOURNAL, and the Board Member of IEEE TRANSACTIONS ON DEVICE AND MATERIALS RELIABILITY.